

Exploring the QCD phase transition in core collapse supernova simulations in spherical symmetry

T. Fischer[†], I. Sagert[‡], M. Hempel[‡], G. Pagliara[‡], J. Schaffner-Bielich[‡],
A. Mezzacappa^{*}, F.-K. Thielemann[†] and M. Liebendörfer[†]

[†]Department of Physics, University of Basel, Klingelbergstrasse 82, 4056 Basel, Switzerland

[‡]Institut für Theoretische Physik, Ruprecht-Karls-Universität, Philosophenweg 16, 69120 Heidelberg, Germany

^{*} Physics Division, Oak Ridge National Laboratory, Oak Ridge, Tennessee 37831-1200, US

Abstract

For finite chemical potential effective models of QCD predict a first order phase transition. In favour for the search of such a phase transition in nature, we construct an equation of state for strange quark matter based on the MIT bag model. We apply this equation of state to highly asymmetric core collapse supernova matter with finite temperatures and large baryon densities. The phase transition is constructed using the general Gibbs conditions, which results in an extended coexistence region between the pure hadronic and pure quark phases in the phase diagram, i.e. the mixed phase. The supernovae are simulated via general relativistic radiation hydrodynamics based on three flavor Boltzmann neutrino transport in spherical symmetry. During the dynamical evolution temperatures above 10 MeV, baryon densities above nuclear saturation density and a proton-to-baryon ratio below 0.2 are obtained. At these conditions the phase transition is triggered which leads to a significant softening of the EoS for matter in the mixed phase. As a direct consequence of the stiffening of the EoS again for matter in the pure quark phase, a shock wave forms at the boundary between the mixed and the pure hadronic phases. This shock is accelerated and propagates outward which releases a burst of neutrinos dominated by electron anti-neutrinos due to the lifted degeneracy of the shock-heated hadronic material. We discuss the radiation-hydrodynamic evolution of the phase transition at the example of several low and intermediate mass Fe-core progenitor stars and illustrate the expected neutrino signal from the phase transition.

1 Introduction

The investigation of the QCD phasediagram via heavy-ion experiments at BNL's RHIC, CERN's LHC and the FAIR facility at GSI poised to explore the properties of QCD matter under extreme conditions. Three of the most important aspects are the behaviour and the position of the critical points in the phase diagram, the phase transition from hadronic matter to quark matter at finite chemical potentials and the properties of the predicted quark phases. In search for these aspects, observations of astronomical objects and astrophysical processes that are assumed to contain quark matter could be helpful. In such favour, Cold and isolated or binary neutrons stars (NS) have long been served as powerful objects to probe the equation of state (EoS) for hadronic as well as for quark matter. In the latter case the NS is called a hybrid star if in addition to the quark core a hadronic envelope is present. The astrophysical processes that leave an isolated NS as the final remnant are core collapse supernovae of low and intermediate mass Fe-core progenitor stars. Naturally the question rises at which stage during the dynamical evolution from a collapsing Fe-core to an isolated NS the thermodynamic conditions are such that the appearance of quark matter is favoured? Even further in the case of a phase transition from hadronic matter to quark matter, which hydrodynamic evolution can be expected and is there a relation to observations? The two intrinsically different scenarios are either during the early post bounce phase when the temperatures are moderately high or during the cooling of the remnant, where deleptonisation causes a temperature decrease and a density increase. The present article discusses the first case due to the critical conditions given by the quark matter EoS, where a relation to the explosion mechanism is explored. Therefore, a detailed study of core collapse supernovae including radiation-hydrodynamics with spectral neutrino transport and a sophisticated EoS for hot and dense asymmetric matter is required to simulate the matter conditions accurately.

The first study of the QCD phase transition in core collapse supernovae was published by Takahara and Sato (1988), suggesting a relation of the multi-peak neutrino signal from supernova 1987A (see Hirata et al. (1988)) to the appearance of quark matter. Using general relativistic hydrodynamics, they modelled the phase transition via a polytropic EoS. Due to the absence of neutrino transport they could neither confirm nor exclude the suggested prediction of a neutrino signal from the phase transition. Additional microphysics was included in the study by Gentile et al. (1993), where general relativistic hydrodynamics is coupled to a description of deleptonisation during the collapse phase of a progenitor star. Applying the MIT-bag model for the description of the quark phase, they find the formation of a (second) shock wave as a direct consequence of an extended co-existence region between the hadronic phase and the quark phase with a significantly smaller adiabatic index. The second shock wave follows and merges with the first shock from the Fe-core bounce after a few milliseconds. However, due to the lack of neutrino transport in the post bounce

phase, they were also not able to confirm the predictions made for a possible neutrino signal from the phase transition. The recent investigation by Nakazato et al. (2008) is based on general relativistic radiation hydrodynamics with spectral three flavour Boltzmann neutrino transport. They investigate very massive progenitors of $\sim 100 M_{\odot}$ which collapse to a black hole. Applying the MIT-bag model for quark matter, the time after bounce for black hole formation is shortened and corresponds to the appearance of quark matter, where the central mass exceeds the maximum stable mass given by the quark EoS.

We follow a similar approach and apply the MIT-bag model for the description of quark matter in general relativistic radiation hydrodynamics simulations, based on spectral three flavor Boltzmann neutrino transport. Our simulations are launched from low and intermediate mass progenitors, where no explosions could be obtained in spherical symmetry. We investigate the dynamical effects and discuss the possibility of an observable in the neutrino signal related to the QCD phase transition.

The manuscript is organised as follows. In §2 we will present the standard core collapse supernova scenario and in §3 we will lay down our neutrino radiation hydrodynamics model including both the hadron and quark EoSs. In §4 we will discuss the appearance of quark matter during the early post bounce phase of core collapse supernovae of intermediate mass Fe-core progenitors and summarise the results in §5.

2 Core collapse supernova phenomenology

The Fe-core of massive progenitor stars in the mass range of $9 - 75 M_{\odot}$ collapse at the final stage of nuclear burning due to photodisintegration and deleptonisation, which reduces the proton-to-baryon ratio given by the electron fraction Y_e . During the collapse, the density and temperature increase. The collapse continues and at about $\rho \simeq 10^{13} \text{ g/cm}^3$ neutrinos are trapped. At nuclear densities of $\rho \simeq 2 - 4 \times 10^{14} \text{ g/cm}^3$, the collapse halts and the central core is highly deleptonised where $Y_e \lesssim 0.3$. The core bounces back and a shock wave forms which travels outwards with positive velocities. The central object formed is a hot and lepton-rich proton-neutron star (PNS). The shock suffers continuously from the dissociation of infalling heavy nuclei into free nucleons and light nuclei. In addition as the shock crosses the neutrinospheres, which relate to the neutrino energy and flavour dependent spheres of the last scattering, additional electron captures release a burst of electron-neutrinos. This deleptonisation burst carries away energy of several 10^{53} erg/s (depending on the progenitor model) on a timescale of $10 - 20 \text{ ms}$. This energy loss turns the expanding shock into a standing accretion shock (SAS) with no significant matter outflow already about 5 ms after bounce.

It has long been investigated to revive the SAS via neutrino reactions, leading to neutrino driven explosions (Bethe and Wilson (1985)). Unfortunately, there have

been no explosions obtained for progenitors more massive than $8.8 M_{\odot}$ (Kitauro et al. (2006), Fischer et al. (2009b)) in spherical symmetry. A possible solution has been suggested and has been explored only recently via multi-dimensional effects such as rotation, convection and the development of known fluid instabilities (see for example Miller et al. (1993), Herant et al. (1994), Burrows et al. (1995) and Janka and Mueller (1996)). Such effects increase the neutrino heating efficiency and help to understand aspherical explosions, see for example Bruenn et al. (2006), Janka et al. (2008) and Marek and Janka (2009).

3 The model

Our core collapse supernova model is originally based on Newtonian radiation hydrodynamics and spectral three flavour Boltzmann neutrino transport, developed by Mezzacappa & Bruenn (1993a-c). It has been extended to solve the general relativistic equations for both, hydrodynamics and radiation transport, as documented in Liebendörfer et al. (2001a,b). Special emphasis has been devoted to accurately conserve energy, momentum and lepton number in Liebendörfer et al. (2004). The following neutrino reactions are considered

$$\begin{aligned}
e^- + p &\leftrightarrow n + \nu_e, \\
e^+ + n &\leftrightarrow p + \bar{\nu}_e, \\
e^- + \langle A, Z \rangle &\leftrightarrow \langle A, Z - 1 \rangle + \nu_e, \\
\nu + N &\leftrightarrow \nu + N, \\
\nu + \langle A, Z \rangle &\leftrightarrow \nu + \langle A, Z \rangle, \\
\nu + e^{\pm} &\leftrightarrow \nu + e^{\pm}, \\
e^- + e^+ &\leftrightarrow \nu + \bar{\nu}, \\
N + N &\leftrightarrow N + N + \nu + \bar{\nu}, \\
\nu_e + \bar{\nu}_e &\leftrightarrow \nu_{\mu/\tau} + \bar{\nu}_{\mu/\tau},
\end{aligned}$$

where $N \in (n, p, \langle A, Z \rangle)$ and $\nu \in (\nu_e, \nu_{\mu/\tau})$. Nuclei are considered via a representative nucleus with average atomic mass number A and charge Z respectively. The calculation of the reaction rates for these reactions is based on Bruenn (1985). N - N -Bremsstrahlung has been implemented following Thompson and Burrows (2001) based on Hannestad and Raffelt (1998). The annihilation of trapped electron neutrino pairs was implemented recently and is documented in Fischer et al. (2009a).

The properties of (nuclear) matter in core collapse supernovae are modelled via an EoS. The two standard (hadronic) EoSs for matter in nuclear statistical equilibrium (NSE) are from Lattimer and Swesty (1991) based on the compressible liquid drop model including surface effects and the EoS from Shen et al. (1998) based on the RMF-approach and Thomas-Fermi approximation. The first one can be applied using the

three different compressibilities 180, 220 and 375 MeV and the low asymmetry energy of 29.3 MeV. It is considered a rather soft EoS and was distributed to the community as a subroutine and recently as a table as well. The EoS contains contributions from electrons and positrons as well as photons. The latter EoS has a significantly larger asymmetry energy of 36.9 MeV as well as a high compressibility of 281 MeV which results in a stiff EoS. It is distributed to the community as a baryon EoS-table. For matter in non-NSE, formerly the approximation of an ideal gas of Si-nuclei was used for the baryon EoS. This leads to an increasingly inaccurate internal energy evolution, especially in long term simulations of explosion models where the explosion shock passes through the different layers of composition given by the progenitor. Recently, a nuclear reaction network has been implemented (see Fischer et al. (2009b)) to be able to handle the nuclear composition of the progenitor more accurately and to include more mass of the progenitor up to the hydrogen envelope (depending on the progenitor model). Additionally, contributions from electrons and positrons as well as photons and ion-ion-correlations (only for non-NSE) are added based on Timmes and Arnett (1999) and Timmes and Swesty (2000).

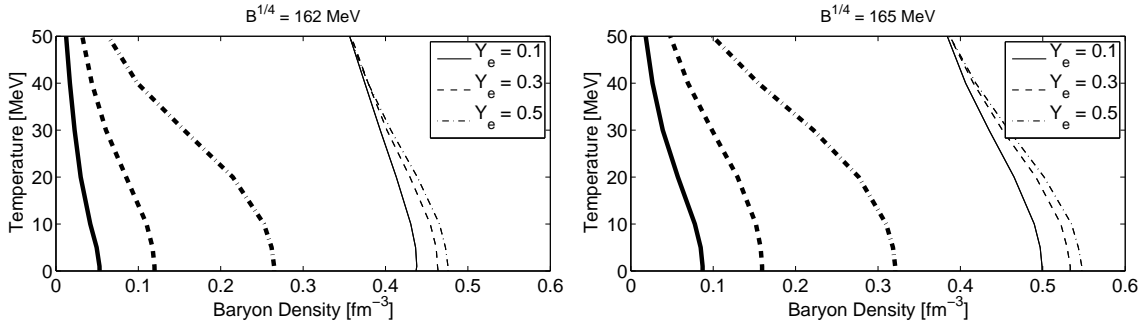


Figure 1: Critical density as a function of the temperature for different electron fractions, for the two quark EoSs (left panel: $B^{1/4} = 162 \text{ MeV}$, right panel: $B^{1/4} = 165 \text{ MeV}$). The lines show the onset (thick) and the endpoint (thin) of the mixed phase from the QCD phase transition from nuclear matter to quark matter.

The quark EoS applied to the present investigation is based on the widely applied MIT bag model. The two values chosen for the bag constant are $B^{1/4} = 162 \text{ MeV}$ and $B^{1/4} = 165 \text{ MeV}$, which leads to a critical density close to nuclear saturation density at low Y_e and finite temperatures and stable maximum gravitational masses of $M = 1.56 M_\odot$ and $M = 1.50 M_\odot$ respectively. This is in agreement with the most precise NS mass measurement of $1.44 M_\odot$ (Hulse-Taylor pulsar). The EoS describes three flavour quark matter where up- and down-quarks are considered to be massless and a strange-quark mass of 100 MeV is assumed. The behaviour of the critical density is illustrated in Fig. 1 for the two values of the Bag constant. For high temperatures and low Y_e , the critical density decreases. This behaviour might change

if a different quark matter description is applied. The mixed phase is constructed using the Gibbs conditions, which leads to an extended co-existence region and a smooth phase transition where the entropy per baryon and the lepton number are conserved.

The nucleon and charge chemical potential as well as the nucleon mass fractions are constructed from the quark chemical potentials and fractions, which are then used to calculate the neutrino reaction rates and the transport based on the hadronic description by Bruenn (1985). Since matter is opaque for neutrinos at densities where quark matter appears, this approximation can be applied as long as the hydrodynamic timescale is shorter than the diffusion timescale for neutrinos to diffuse out of the PNS. This is the case for the post bounce scenario considered here, where the hydrodynamic timescale is 1 – 100 ms and the diffusion timescale is of the order seconds. In addition, the timescale to establish β -equilibrium is much shorter than the hydrodynamic and the diffusion timescales. Hence, β -equilibrium is obtained instantaneously for quark matter.

4 The QCD phase transition during the early post bounce phase

The appearance of quark matter in core collapse supernova simulations is monitored using the quark matter volume fraction x_Q , defined as follows

$$x_Q = \begin{cases} 0 & \text{hadronic matter,} \\]0, 1[& \text{mixed phase,} \\ 1 & \text{quark phase.} \end{cases}$$

This is a standard procedure in nuclear physics where a transition between two different phases is constructed based on two different nuclear physics descriptions. The conditions for the onset of the mixed phase as illustrated in Fig. 1 (thick lines) are already reached at core bounce for the 10, 13 and 15 M_\odot progenitor models from Woosley et al. (2002) under investigation. However, the quark fraction reduces again after bounce due to the density decrease in the expanding regime. Only when the expanding bounce shock stalls and turns into the SAS, the continued mass accretion causes the central density to increase again. The quark fraction rises on a timescale depending on the mass accretion rate and is related to the compression behaviour of the central PNS given by the EoS.

The adiabatic index reduces for matter in the mixed phase. Consequently, the smaller compressibility results in a higher central density for matter in the mixed phase during the post bounce accretion phase on a timescale of 100 ms. The higher central density results in a different degeneracy due to the different β -equilibrium, where matter is found to be more neutron rich reducing the electron fraction below

$Y_e = 0.25$. The additional loss of electron pressure support accelerates the post bounce compression of the central PNS and favours even higher central densities.

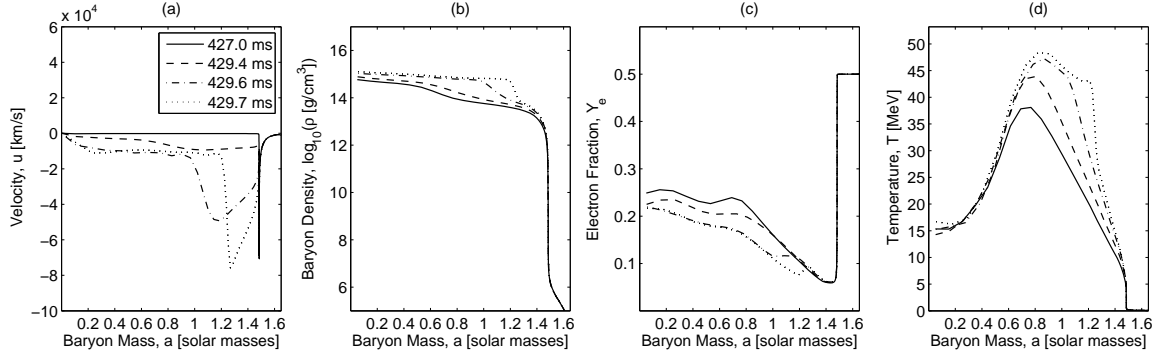


Figure 2: Selected hydrodynamic variables during the QCD phase transition for several post bounce times.

When a certain amount of mass of the PNS is converted into the mixed phase, typically $\sim 0.8 M_{\odot}$, the reduced adiabatic index for matter in the mixed phase causes the PNS to become gravitationally unstable and contract. The contraction is illustrated in Fig. 2 and proceeds into a supersonic adiabatic collapse. Due to the contraction, density and temperature increase which results in an increased degeneracy and hence the electron fraction reduces (see Fig. 2 graphs (b) and (c)). The collapse halts as a reasonable amount of matter (depending on the progenitor) inside the PNS is converted into the pure quark phase via compression and the EoS stiffens again due to the increased adiabatic index. A stagnation wave forms which propagates outwards and turns into a shock wave at the sonic point. This scenario differs from the bounce of the collapsing Fe-core, where the forming shock wave travels outwards with positive velocities immediately after its formation due to the overshooting of the hydrostatic equilibrium configuration. Here, the forming shock wave is not related to a matter outflow and can be considered as a pure accretion shock at the moment of its formation and shortly after. This accretion shock propagates outwards because the thermal pressure behind the shock is much larger than the ram pressure ahead of the shock. The large thermal pressure behind the shock corresponds to the converted hadrons into quarks since the shock spatially separates mixed and hadronic phases. As soon as the expanding accretion shock inside the PNS reaches the PNS surface, it is accelerated along the decreasing density and detaches from the mixed phase. This behaviour as well as selected hydrodynamic variables are illustrated in Fig. 3 (left panel). This scenario is again different from the early post bounce behaviour of the stalling bounce shock - since the bounce shock suffers from the dissociation of infalling heavy nuclei, matter falling onto the second shock is already dissociated and the nucleons are only shifted to higher Fermi levels. In this sense the second

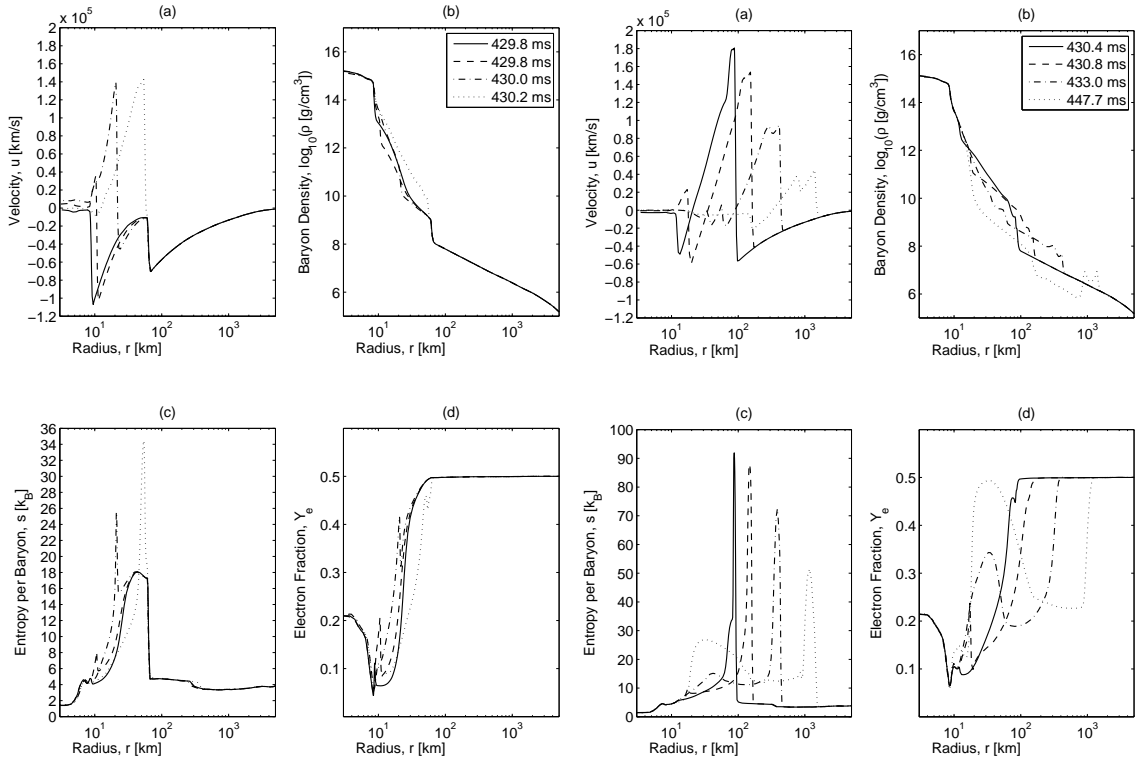


Figure 3: Selected hydrodynamic variables after the QCD phase transition for several post bounce times, illustrating the initial (left panel) and the proceeding (right panel) explosion phases.

shock wave can accelerate quasi-freely. Due to the large density decrease at the PNS surface over several orders of magnitude from 10^{15} to 10^9 g/cm³ (see Fig.3 (b)), the expanding shock wave reaches relativistic velocities of the order $\sim 50\%$ the vacuum speed of light (see Fig.3 (a)). In other words, not only general relativistic effects are important for the hydrodynamics equations as well as for the neutrino transport in the presence of strong gravitational fields inside the PNS but also kinetic relativistic effects become important due to the high matter outflow velocities.

The previously shock heated and highly deleptonised material is accumulating onto the second expanding shock, where it is shock heated again and the degeneracy reduces such that β -equilibrium is established at a larger value of the electron fraction (see Fig.3 (d)). This lifted degeneracy relates to a large fraction of electron-antineutrinos that are emitted but still can not escape because the matter conditions correspond to the trapping regime. Only when the second shock propagates across the neutrinospheres, the additionally produced neutrinos can escape which becomes observable in the neutrino spectrum as a second neutrino burst. It is accompanied by a significant increase of the mean neutrino energies. This burst is then dominated

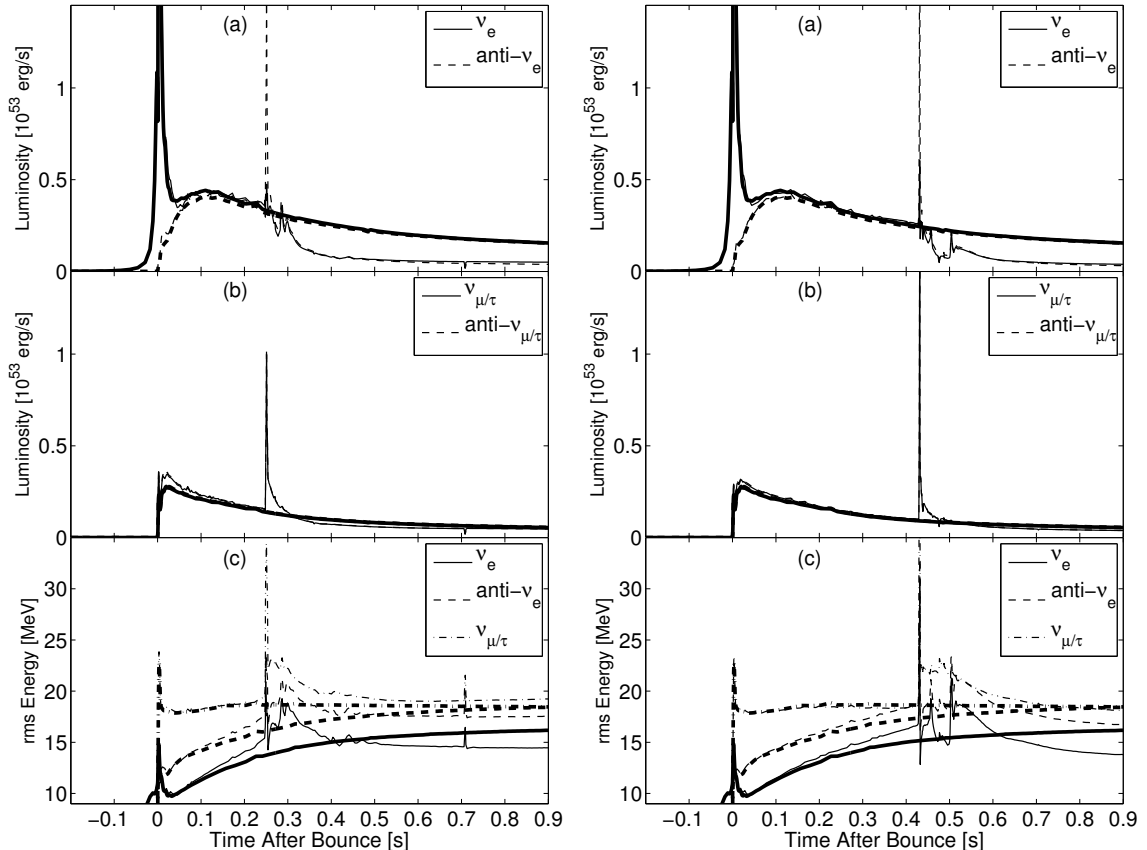


Figure 4: Neutrino Luminosities and mean neutrino energies for both quark EoSs (thin lines), i.e. $B^{1/4} = 162$ MeV (left panel) and $B^{1/4} = 165$ MeV (right panel), in comparison to the pure hadronic EoS from Shen et al. (1998) (thick lines) for the $10 M_{\odot}$ progenitor model under investigation.

by electron-antineutrinos due to the lifted degeneracy, again different from the deleptonisation burst at bounce which is only due to electron-neutrinos (see Fig. 4). The post bounce time of the second burst contains correlated information about the contraction behaviour of the central PNS, which in turn depends on the (compressibility and asymmetry energy of the) EoS for hadronic matter and the progenitor model, as well as the critical conditions for the QCD phase transition. For the same progenitor model, a low critical density (i.e. the small bag constant) corresponds to an early phase transition. The critical conditions for the quark matter phase transition can be related to the delay of the second neutrino burst. This delay depends on the central density increase given by the mass accretion rate and the hadronic EoS.

The expanding second shock wave finally merges with the first shock, which remained unaffected by the happenings inside the PNS at ~ 100 km, and an explosion

is obtained. After the explosion has been launched, the luminosities and mean neutrino energies decay. In addition, a region of neutrino cooling develops between the expanding explosion ejecta and the PNS surface at the centre. This can be seen in Fig. 3 at the velocity profiles in the graphs (a) (right panel), where initial mass inflow develops to an additional weak accretion shock. This expanding and contracting shock determines the oscillating luminosity behaviour after the second neutrino burst, illustrated in Fig. 4. The following dynamical evolution of the explosion ejecta can be approximated by an adiabatic expansion. However the later appearance of the neutrino driven wind and the related dynamic impact to the composition of the ejecta will have to be analysed consistently in explosive nucleosynthesis investigations.

5 Summary

Table 1: Selected properties of the PNSs for the different progenitor models under investigation.

Prog.	bag constant	t_{pb}	M_{PNS}	E_{expl}	ρ_c	T_c	Y_e
[M_{\odot}]	[MeV]	[ms]	[M_{\odot}]	[10^{51} erg]	[10^{14} g/cm ³]	[MeV]	
10	162	248	1.434	0.361	6.6069	13.14	0.2343
10	165	429	1.482	1.080	5.8884	15.33	0.2488
13	162	241	1.467	0.146	6.4565	13.32	0.2335
13	165	431	1.498	0.323	5.6234	15.55	0.2462
15	162	209	1.608	0.420	6.7608	14.10	0.2262
15	165	330 ¹	1.700	unknown ²	5.4954	15.33	0.2479

¹ time of black hole formation

² black hole formation before positive explosion energies are achieved

The results of this first investigation of the QCD phase transition in core collapse supernova simulations of low and intermediate mass Fe-core progenitor stars is summarised in Table 5. The simulations are launched from progenitor stars of 10, 13 and 15 M_{\odot} from Woosley et al. (2002). The post bounce times t_{pb} correspond to the appearance of the second neutrino burst in the spectra and the PNS masses M_{PNS} are taken at the electron-neutrinospheres at some late post bounce times when the simulations are stopped. The central thermodynamic conditions, density ρ_c , temperature T_c and electron fraction Y_e , correspond to the initial PNS collapse. A special model is the 15 M_{\odot} progenitor using $B^{1/4} = 165$ MeV, where the maximum mass is reached shortly after the QCD phase transition. Hence, the PNS collapses to a black hole before the already formed second shock is accelerated to positive velocities. Due to our co-moving coordinate choice, no stable solution for the equations of energy and

momentum conservation can be obtained and t_{pb} determines the time of black hole formation after bounce.

The significant softening of the EoS for matter which is in the mixed phase causes the PNS to collapse. As a direct consequence of the softening of the EoS for matter which reaches the pure quark phase, a second shock wave forms. The second shock accelerates and finally merges with the first shock and launches an explosion. The explosion energies E_{expl} are give in Table 5. This mechanism was explored and found to even produce explosions in spherical symmetry using general relativistic radiation hydrodynamics based on spectral three-flavour Boltzmann neutrino transport, where otherwise no explosion could be obtained. The explosion energies in Table 5 are evaluated at some late post bounce times when the simulations are stopped and might have not yet converged to the final value of the explosion energy. The simulations will have to be carried out longer. However, moderate explosion energies of $\simeq 10^{51}$ erg could be found for the $10 M_{\odot}$ model using $B^{1/4} = 165$ MeV (i.e. the later phase transition), otherwise lower explosion energies are obtained. The explosion energies might be shifted to larger values when multi-dimensional effects such as convection and rotation are taken into account.

The second shock forms in the high density regime where neutrinos are fully trapped. Hence, no direct observational identification of the QCD phase transition can be found in the emitted neutrino spectra. It would be different if analysing the emitted gravitational waves directly from the phase transition (Abdikamalov et al. (2009)). Unfortunately, gravitational waves have proven difficult to detect. Nevertheless, an indirect observation can be found in the emitted neutrino spectra. A second neutrino burst is released when the second shock, formed during the PNS collapse, propagates over the neutrinospheres. This second burst is, due to the lifted degeneracy of the shock heated hadronic material, dominated by electron-antineutrinos. The burst is accompanied by a significant increase of the mean neutrino energies which might become resolvable by neutrino detector facilities such as Super-Kamiokande for a future Galactic core collapse supernova explosion if quark matter appears.

One of the most important observations from supernova explosions is the composition of the ejecta, which is determined by explosive nucleosynthesis investigations and are model dependent (see for example Fröhlich et al. (2006a-c)). Of special interest is the production of heavy elements for which rapid neutron captures (r -process) in supernova explosion models have long been investigated (see for example Woosley and Baron (1992), Woosley et al. (1994), Wittl et al. (1994), Otsuki et al. (2000), Thompson et al. (2001), Wanajo et al.(2006a,b), Arcones et al. (2007), Panov and Janka (2009)). The abundances are calculated via post processing of mass trajectories from explosion models and compared with the well known solar abundances. Unfortunately, the very recent neutrino driven explosion models fail to provide conditions favourable for the r -process, which are high entropies per baryon, a fast expansion timescales and generally neutron rich material. Especially the latter

aspect is a subject of research. Although the explosion models achieved via the QCD phase transition of the present article have to be analysed consistently with respect to explosive nucleosynthesis, a reasonable amount of ejected matter is found to be neutron-rich where $Y_e \simeq 0.35 - 0.45$. In addition, moderate entropies per baryon and a fast expansion timescale are obtained. The conditions found may indeed be favourable for the r -process.

Acknowledgment

The project was funded by the Swiss National Science Foundation grant. no. PP02-106627/1 and 200020-122287 and the Helmholtz Research School for Quark Matter Studies, the Italian National Institute for Nuclear Physics, the Graduate Program for Hadron and Ion Research (PG-HIR), the Alliance Program of the Helmholtz Association (HA216/EMMI) and the DFG through the Heidelberg Graduate School of Fundamental Physics. The authors are additionally supported by CompStar, a research networking program of the European Science Foundation, and the Scopes project funded by the Swiss National Science Foundation grant. no. IB7320-110996/1. A.Mezzacappa is supported at the Oak Ridge National Laboratory, which is managed by UT-Battelle, LLC for the U.S. Department of Energy under contract DE-AC05-00OR22725.

References

- Abdikamalov, E. B.; Dimmelmeier, H.; Rezzolla, L. and Miller, J. C. 2009, *Mon. Not. R. Astron. Soc.*, 392, 52
- Arcones, A.; Janka, H.-Th.; and Scheck L. 2007, *A&A*, 467, 1227
- Bethe, H. A. and Wilson, J. R. 1985, *ApJ*, 295, 14
- Bruenn, S. W. 1985, *ApJS*, 58, 771
- Bruenn, S. W.; Dirk, C. J.; Mezzacappa, A.; Hayes, J. C.; Blondin, J. M.; Hix, W. R. and Messer, O. E. B. 2006, *Journal of Physics Conference Series*, 46, 393
- Burrows, A.; Hayes, J. C. and Fryxell, B. A. 1995, *ApJ*, 450, 830
- Fischer, T.; Whitehouse, S. C.; Mezzacappa, A.; Thielemann, F.-K. and Liebendörfer, M. 2009a *A&A*, 499, 1
- Fischer, T.; Whitehouse, S. C.; Mezzacappa, A.; Thielemann, F.-K. and Liebendörfer, M. 2009b, *ArXiv e-prints* 0908.1871

- Fröhlich, C.; Hauser, P.; Liebendörfer, M.; Martínez-Pinedo, G.; Thielemann, F.-K.; Bravo, E.; Zinner, N. T.; Hix, W. R.; Langanke, K.; Mezzacappa, A. and Nomoto; K. 2006a *ApJ*, 637, 415
- Fröhlich, C.; Hix, W. R.; Martínez-Pinedo, G.; Liebendörfer, M.; Thielemann, F.-K.; Bravo, E.; Langanke, K. and Zinner, N. T. 2006b, *New Astronomy Review*, 50, 496
- Fröhlich, C.; Martínez-Pinedo, G.; Liebendörfer, M.; Thielemann, F.-K.; Bravo, E.; Hix, W.-R.; Langanke, K. and Zinner, N. T. 2006c *Physical Review Letters*, 96 (14), 142502
- Gentile, N. A.; Aufderheide, M. B.; Mathews, G. J.; Swesty, F. D. and Fuller, G. M. 1993, *ApJ*, 414, 701
- Hannestad, S. and Raffelt, G. 1998, *ApJ*, 507, 339
- Herant, M.; Benz, W.; Hix, W. R.; Fryer, C. L. and Colgate, S. A. 1994, *ApJ*, 435, 339
- Hirata, K. S.; Kajita, T.; Koshiba, M.; Nakahata, M.; Oyama, Y.; Sato, N.; Suzuki, A.; Takita, M.; Totsuka, Y.; Kifune, T.; Suda, T.; Takahashi, K.; Tanimori, T.; Miyano, K.; Yamada, M.; Beier, E. W.; Feldscher, L. R.; Frati, W.; Kim, S. B.; Mann, A. K.; Newcomer, F. M.; van Berg, R.; Zhang, W. and Cortez, B. G. 1988, *PRD*, 38, 448
- Janka, H.-Th. and Mueller, E. 1996, *A&A*, 306, 167
- Janka, H.-Th.; Marek, A.; Müller, B. and Scheck, L. 2008, In C. Bassa, Z. Wang, A. Cumming, and V. M. Kaspi, editors, *40 Years of Pulsars: Millisecond Pulsars, Magnetars and More*, volume 983 of *American Institute of Physics Conference Series*, 369
- Kitaura, F. S.; Janka, H.-Th. and Hillebrandt, W. 2006, *A&A*, 450, 345
- Lattimer, J. M. and Swesty, D. F. 1991, *Nuclear Physics A*, 535, 331
- Liebendörfer, M.; Mezzacappa, A.; Thielemann, F.-K.; Messer, O. E. B.; Hix, W. R. and Bruenn, S. 2001a, *PRD*, 63, 103004
- Liebendörfer, M.; Mezzacappa, A. and Thielemann, F.-K. 2001b, *PRD*, 63, 104003
- Liebendörfer, M.; Messer, O. E. B.; Mezzacappa, A.; Bruenn, S. W.; Cardall, C. Y. and Thielemann, F.-K. 2004, *ApJS*, 150, 263
- Marek, A. and Janka, H.-Th. 2009, *ApJ*, 694, 664

- Mezzacappa, A. and Bruenn, S. W. 1993a, *ApJ*, 405, 637
- Mezzacappa, A. and Bruenn, S. W. 1993b, *ApJ*, 405, 669
- Mezzacappa, A. and Bruenn, S. W. 1993c, *ApJ*, 410, 740
- Miller, D. S.; Wilson, J. R. and Mayle, R. W. 1993, *ApJ*, 415, 278
- Nakazato, K.; Sumiyoshi, K. and Yamada, S. 2008, *PRD*, 77 (10), 103006
- Otsuki, K.; Tagoshi, H.; Kajino, T. and Wanajo, S. Y. 2000, *ApJ*, 533, 424
- Panov, I. and Janka, H.-Th. 2009, *A&A*, 494, 829
- Shen, H.; Toki, H.; Oyamatsu, K. and Sumiyoshi, K. 1998, *Nuclear Physics A*, 637, 435
- Takahara, M. and Sato, K. 1988, *ApJ*, 335, 301
- Thompson, T. A. and Burrows, A. 2001, *Nuclear Physics A*, 688, 377
- Thompson, T. A.; Burrows, A. and Meyer, B. S. 2001, *ApJ*, 562, 887
- Timmes, F. X. and Arnett, D. 1999, *ApJS*, 125, 277
- Timmes, F. X. and Swesty, F. D. 2000, *ApJS*, 126, 501
- Wanajo, S. 2006a, *ApJ*, 647, 1323
- Wanajo, S. 2006b, *ApJL*, 650, L79
- Witti, J.; Janka, H.-Th. and Takahashi, K. 1994, *A&A*, 286, 841
- Woosley, S. E. and Baron, E. 1992, *ApJ*, 391, 228
- Woosley, S. E.; Wilson, J. R.; Mathews, G. J; Hoffman, R. D. and Meyer, B. S. 1994, *ApJ*, 433, 229
- Woosley, S. E.; Heger, A. and Weaver, T. A. 2002, *Reviews of Modern Physics*, 74, 1015